Received: 23 January 2020 | Accepted: 4 February 2020

DOI: 10.1002/maco.202011541

ARTICLE

Materials and Corrosion

Chloride-induced steel corrosion in alkali-activated fly ash mortar: Increased propensity for corrosion initiation at defects

Gregor J. G. Gluth | **Gino Ebell** | **Petr Hlaváček** | **Jürgen Mietz**

Dedicated to Professor Dr-Ing. Michael Raupach on the occasion of his 60th birthday

Bundesanstalt für Materialforschung und -prüfung (BAM), Berlin, Germany

Correspondence
Gregor J. G. Gluth, Division 7.4 Technology of Construction Materials, Bundesanstalt für Materialforschung und -prüfung (BAM), Unter den Eichen 87, 12205 Berlin, Germany.
Email: gregor.gluth@bam.de

Funding information
AiF, Grant/Award Number: 18910 N/1

Abstract

Chloride contents at the steel–mortar interface that initiate steel corrosion were determined for carbon steel in alkali-activated fly ash mortar for three different exposure conditions: exposure to 1 M NaCl solution; leaching in deionized water and then exposure to 1 M NaCl solution; and leaching in deionized water, aging in air at 20°C and natural CO_2 concentration, and then exposure to 1 M NaCl solution. For comparison, a Portland cement mortar, exposed to 1 M NaCl solution, was studied. The median values of the corrosion-initiating chloride contents (average over the full length of the rebar) in the alkali-activated fly ash mortar varied between 0.35 and 1.05 wt% Cl with respect to binder, consistently lower than what was obtained for the Portland cement mortar, but with no clear trend regarding the exposure conditions. For most of the alkali-activated fly ash mortar specimens, preferential corrosion at the connection between the working electrode and the external measurement setup was observed, while preferential corrosion did not occur for the Portland cement mortar. Scanning electron microscopy and auxiliary experiments in synthetic solutions indicated that this behavior was caused by inhomogeneities at the steel–mortar interface in the alkali-activated mortar, likely due to its peculiar rheological properties in the fresh state.

KEYWORDS

alkali-activated materials, chloride, reinforcement corrosion, steel–concrete interface

1 | INTRODUCTION

Chloride-induced steel corrosion in reinforced concrete structures is one of the most important deterioration mechanisms limiting their service life.[1] Chloride ions that reach the steel–concrete interface cause, above a certain concentration, depassivation and stable pitting corrosion of the steel,[2–5] eventually leading to significant loss of reinforcement cross-sectional area and potentially to a collapse of the structure. The time to the onset of chloride-induced reinforcement corrosion is thus determined by the rate of chloride ingress into the concrete

and the critical chloride content (c_{crit}; also referred to as chloride threshold value) of the steel/concrete system.

While extensive data regarding the critical chloride content in concretes and mortars based on Portland cement and blended cement have been compiled,[6–8] much less data in this regard are available for concretes or mortars based on alkali-activated binders.[9] Early work showed that carbon steel in chloride-free alkali-activated fly ash mortars attains a passive state and indicated that chloride contents up to 0.4 wt% with respect to binder (wrtb) do not cause steel corrosion in these mortars.[10] The authors of a more recent study[11] concluded that the critical chloride content for the onset of steel corrosion in alkali-activated fly ash mortars is in the range 1–1.7 wt% wrtb. However, the data presented in that paper strongly suggests an upper bound of 0.5 wt% wrtb as the c_{crit} for the tested materials (chloride content at the rebar after 10 days, while depassivation occurred apparently between 1 and 9 days of exposure). The same group presented additional data[12] that suggest even lower critical chloride contents for alkali-activated fly ash mortars under carbonation and chloride ingress, with chloride contents of ~0.1 wt% wrtb around the time of corrosion initiation, as judged by a decrease of polarization resistance and corrosion potential. In a subsequent study, critical chloride contents in the range ~0.2–0.7 wt% wrtb were obtained for mortars based on alkali-activated slag/fly ash blends, with higher c_{crit} generally observed for mortars with higher fly ash contents in the binder.[13]

Thus, reported c_{crit} for mortars based on alkali-activated fly ashes (or fly ash-dominated alkali-activated binders) vary considerably, and the interpretation of the underlying data sometimes appears to be equivocal. Importantly, experiments in synthetic pore solutions have shown that c_{crit} in alkali-activated materials with low Ca content ("low-Ca alkali-activated materials") is strongly dependent on the pH of the pore solution,[14] which may explain some of the discrepancies in the literature. Another factor that influences the results of studies of the critical chloride content for all types of binder is the size of the studied specimens (i.e., exposed steel surface area).[15] In addition, recent work has highlighted the importance of the redox conditions in the pore solution of alkali-activated binders, which is mainly controlled by sulfides from slag in the binder, for chloride-induced corrosion of embedded steel.[9,16]

In the present study, chloride contents that initiate corrosion of steel rebars in alkali-activated fly ash mortar, exposed to leaching, aging, and chloride (1 M NaCl solution), were determined. For comparison, a Portland cement mortar was tested. The transition from a passive state to an active state of the steel was followed using open-circuit potential measurements and galvanostatic pulse measurements. After corrosion initiation, the average chloride contents at the steel–mortar interface were determined and the rebars visually inspected. In addition, the steel–mortar interface in companion specimens was studied by scanning electron microscopy (SEM), and auxiliary corrosion experiments in synthetic solutions were performed. The obtained results highlight the importance of an additional complicating factor for chloride-induced steel corrosion in alkali-activated mortars and concretes and pertinent test methods, namely, a potentially regular formation of inhomogeneities at the steel–mortar or steel–concrete interface.

2 | MATERIALS AND METHODS

2.1 | Starting materials and specimens

Alkali-activated fly ash mortar was produced from 580 kg/m^3 hard coal fly ash (chemical composition given in Table 1; median particle size $d_{50} = 12.9\ \mu m$), 319 kg/m^3 sodium silicate solution (18.4% Na_2O, 20.0% SiO_2) as activator and 1,333 kg/m^3 quartz sand (0.1–4 mm). The alkali-activated fly ash mortar will be referred to as "FA" in the designations of the mortar-exposure combinations below.

For comparison, a Portland cement mortar was produced from 606 kg/m^3 Portland cement (CEM I 42.5R; chemical composition given in Table 1), 273 kg/m^3 water (i.e., $w/c = 0.45$) and 1,304 kg/m^3 quartz sand (0.1–4 mm). The Portland cement mortar will be referred to as "CEM" in the designations of the mortar-exposure combinations below.

Ribbed BSt 500 carbon steel rebars with a nominal diameter of 10 mm and a length of 120 mm were embedded in the mortar prisms for the corrosion investigations. First, stainless-steel (1.4576) wires with a diameter of 2 mm were welded to the ends of the rebars, the assemblage cleaned by grit blasting with corundum grit, and then installed in the 40 × 40 × 160 mm prism molds into predrilled locating holes (Figure 1).

TABLE 1 Chemical composition of the binder starting materials (in wt%)

	SiO_2	Al_2O_3	Fe_2O_3	TiO_2	CaO	MgO	Na_2O	K_2O	SO_3	LOI
Fly ash	57.4	17.5	7.0	1.3	7.4	0.6	0.5	1.0	0.8	4.1
Portland cement	19.6	4.6	2.5	0.2	64.3	2.2	0.2	0.9	2.6	2.8

Abbreviation: LOI, loss on ignition.

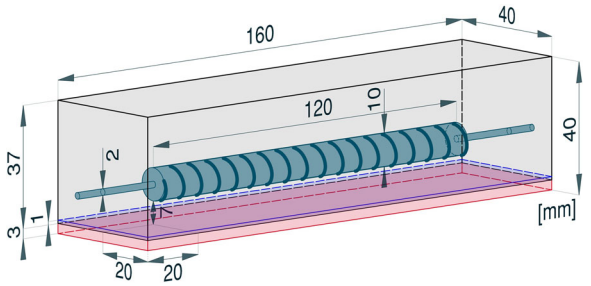

FIGURE 1 Sample geometry used in the corrosion experiments. The 3-mm thick bottom layer of the mortar sample (transparent orange) was ground off before testing to reduce the mortar cover layer. The 1-mm thick layer above the latter (transparent blue) represents the volume immersed in the 1 M NaCl solution during testing [Color figure can be viewed at wileyonlinelibrary.com]

The mortars were mixed in a 30-dm^3 rotating pan mixer for 4 min, subsequently cast into the molds with the pre-installed rebars and the molds vibrated for 30 s. In addition, mortar prisms with the same external dimensions but without embedded steel were produced for strength testing and determination of their porosity (results are shown in Table 2). The alkali-activated fly ash mortar specimens were heat-cured at 80°C and a relative humidity (RH) of 80% for 24 hr. The Portland cement mortar specimens were cured in the covered molds at 23°C for 1 day, subsequently removed from the molds and then cured above open water in a sealed box for 28 days. After curing, the specimens with embedded steel were ground to remove a 3-mm layer at the bottom (Figure 1) to reduce the mortar cover of the steel rebar to a thickness of 7 mm. Subsequently, the prisms were cleaned in an ultrasonic water bath and then cured at 20–23°C/50–65% RH for either additional 14–28 days (alkali-activated fly ash mortar) or additional 106 days (Portland cement mortar).

2.2 | Exposure conditions and analytical methods

After curing, the mortar specimens with embedded steel rebars were exposed to one of the following three exposure schemes:

TABLE 2 Compressive strength (f_c), flexural strength (f_t), and total porosity (φ) of the mortars

	f_c (MPa)	f_t (MPa)	φ (vol%)
FA	80.9 ± 2.0	7.8 ± 0.4	21.7 ± 0.2
CEM	70.6 ± 1.9	7.1 ± 0.3	14.3 ± 0.3

Note: Mean values from at least three measurements; standard deviations are given after the ± sign.

- Soaking in tap water (partially immersed) for 6 days; partial immersion in 1 M NaCl solution until depassivation of the steel was detected (exposure scheme denoted "Cl").
- Leaching in deionized water (fully immersed) for 31 days; partial immersion in 1 M NaCl solution until depassivation of the steel was detected (exposure scheme denoted "L-Cl").
- Leaching in deionized water (fully immersed) for 31 days; aging at 20°C and 65% RH for 70 days; soaking in tap water (partially immersed) for 6 days; partial immersion in 1 M NaCl solution until depassivation of the steel was detected (exposure scheme denoted "L-A-Cl").

At predetermined intervals, measurements of the open-circuit potential (E_{corr}) and galvanostatic pulse measurements[17,18] for the determination of the polarization resistance (R_p) and the ohmic resistance (R_{el}) were performed to follow the transition of the embedded steel from the active state to the passive state.

For the galvanostatic pulse measurements, the mortar specimens were transferred to a three-electrode setup, in which they were partially immersed in tap water (Figure 2). Specimens that were measured during leaching or soaking periods were allowed to dry in air for ~24 hr on a lab bench before being installed in the three-electrode measurement cell; specimens that were measured during aging or chloride exposure periods were installed in the cell immediately after removal from the exposure conditions. The counter electrode of the setup was a mixed-metal oxide mesh; a Ag/AgCl$_{(sat.)}$ electrode served as the reference electrode. The measurements were performed using a Gamry Instruments Potentiostat/Galvanostat/ZRA Interface 1000 device, which

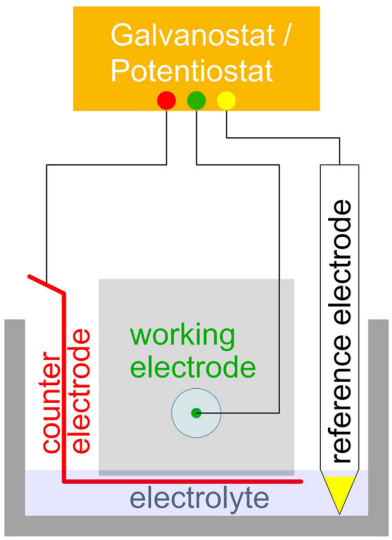

FIGURE 2 Schematic of the three-electrode setup used for electrochemical measurements [Color figure can be viewed at wileyonlinelibrary.com]

was connected to the working electrode (steel rebar) via the welded stainless-steel wires. After stabilization and recording of E_{corr}, the ohmic resistance and the polarization resistance were determined under the following conditions: $\Delta t = 20$ s; $I = \pm(5...50)$ μA. Since there was always good agreement between the results obtained with anodic and cathodic pulses, only those obtained with anodic pulses will be reported below. Immediately after the measurements in the three-electrode cell, the specimens were transferred back to exposure conditions. Additional measurements of E_{corr} were conducted approximately daily during chloride exposure while the specimens were immersed in the 1 M NaCl solution with a voltmeter that was electrically connected to the rebar via the welded stainless-steel wires, using a $Ag/AgCl_{(sat.)}$ reference electrode.

After corrosion initiation of a specimen was identified by a significant decrease of E_{corr} and R_p (see Section 3.1), the mortar prism was split along a plane through the steel rebar, parallel to the face that was immersed in the 1 M NaCl solution. Photographs were taken of the steel–mortar interfaces and the rebar. Subsequently, powder for determination of the total chloride content was ground off from the original steel–mortar interface in the "bottom" piece of the mortar prisms (i.e., in the part closer to the face that was immersed in the 1 M NaCl solution), along the full length of the original rebar position.

Digestion of the powders for determination of the chloride content was done by first drying the sample powder at 105°C, and then dissolving the powder in nitric acid (1 + 4), keeping the solution at a temperature just below boiling for 3 min, precipitation of hydroxides by adding aqueous ammonia to the solution, and filtrating the solution. The thus-prepared solutions were subjected to analysis of the Cl content by potentiometric titration. All chloride contents were recalculated as wt% Cl wrtb, where the binder includes the fly ash and the solids (Na_2O and SiO_2) in the activator solution for the alkali-activated mortar and is equal to the cement for the Portland cement mortar.

2.3 | Corrosion experiments in synthetic solutions

For experiments in solutions, ribbed carbon steel (BSt 500) rebars as for the mortar experiments, but with a length of 30 mm, with 2-mm diameter stainless-steel (1.4576) wires welded to their ends, prepared and grit-blasted as the rebars for the mortar experiments, were used. In addition, single stainless-steel (1.4576) wires with a diameter of 2 mm and a length of 30 mm were tested in solution. The specimens were first immersed in a 1 M NaOH solution and their open-circuit potential (E_{corr}) recorded. After 2 hr, the samples were polarized in anodic direction at a rate of 1 mV/s, starting at −50 mV from E_{corr}, and the resulting current density–potential curves recorded. Three of the carbon steel specimens with welded wires were left in the 1 M NaOH solution for an additional 24 hr and then transferred to a 1.7 M NaCl/1 M NaOH solution. After waiting for approximately 5 min, current density–potential curves were recorded in the chloride-containing solution using the same measurement parameters as before.

All electrochemical measurements in solution were performed with a Gamry Instruments Potentiostat/Galvanostat/ZRA Interface 1000 device, using a mixed-metal oxide mesh as counter electrode and a $Ag/AgCl_{(sat.)}$ electrode as the reference electrode. The concentration of the starting (passivating) solution and the background of 1 M NaOH for the chloride-containing solution was chosen to approximate the pore solution composition of cured alkali-activated fly ashes.[19,20]

2.4 | Scanning electron microscopy

Investigation of the steel–mortar interface was performed using SEM for three alkali-activated fly ash mortar specimens and two Portland cement mortar specimens. Mortar prisms with embedded rebar produced and cured as the specimens for chloride exposure were stored at 20°C/65% RH until required for testing. Sections were obtained by cutting with a water-cooled diamond saw at a distance of ~20 mm away from the end face of the prism, that is, in the immediate vicinity of the joint between the rebar and the stainless-steel wire, and within ± 10 mm of the middle between the end faces of the prism, that is, in the central region of the prism.

Subsequently, the specimens were dried at 40 mbar and 40°C, vacuum-impregnated with epoxy resin and then ground and polished with diamond spray down to a particle size of 1 μm. The polished samples were fixed on adhesive double-coated carbon conductive tabs, sputter-coated with a ~15-nm thick gold layer and then analyzed with a Zeiss EVO MA 10 scanning electron microscope in backscattered electron (BSE) mode at an acceleration voltage of 10 kV.

3 | RESULTS AND DISCUSSION

3.1 | Open-circuit potential, polarization resistance, and ohmic resistance

After curing, all specimens exhibited open-circuit potentials (E_{corr}) in the range 0–100 mV and polarization resistances (R_p) in the range 60–90 kΩ·cm^2 (Figures 3–6). These values are in line with previous observations and

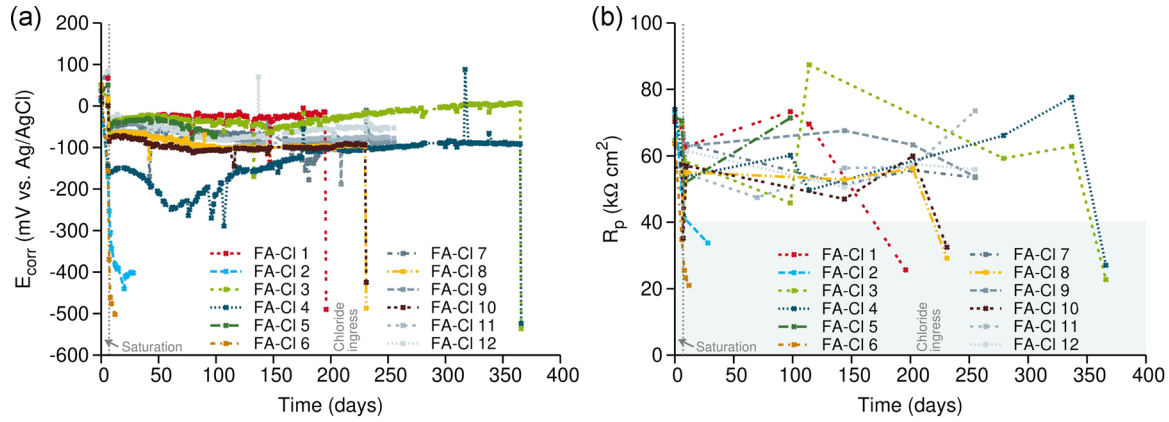

FIGURE 3 (a) Evolution of the open-circuit potential E_{corr} and (b) the polarization resistance R_p of the steel in alkali-activated fly ash mortar exposed to chloride ("Cl") [Color figure can be viewed at wileyonlinelibrary.com]

indicate that in both materials, alkali-activated fly ash mortar and Portland cement mortar, the steel had attained the passive state during curing.[9,21] The ohmic resistances (R_{el}) after curing were 500–600 Ω for the Portland cement mortar specimens and ~400 Ω for the alkali-activated fly ash mortar (Figures S1–S4), indicating a finer pore structure and possibly a lower ionic strength of the pore solution in the Portland cement mortar.

Leaching of the alkali-activated fly ash mortar (FA-L-Cl and FA-L-A-Cl; Figures 4 and 5) caused an increase of E_{corr} by approximately 100 mV, which can be explained by loss of sodium ions from the mortar and the concomitant decrease of the pH of the pore solution (cf. References[19,20]). During the leaching period, R_p exhibited some fluctuations but did not change in a systematic manner, indicating that leaching did not induce significant changes in the condition of the steel surface. This is in accord with previous work,[21] which demonstrated that carbon steel reinforcement in the alkali-activated fly ash mortar remains in the passive state during severe leaching for more than 300 days. As expected, leaching led to a significant reduction of R_{el} by ~250 Ω (Figures S2 and S3), related to the loss of alkali and hydroxyl ions from the pore solution.

Aging at 65% RH of the specimens in the FA-L-A-Cl series caused a substantial increase of R_{el} (Figure S3), which is related to the loss of water from the mortar during this period, that is, the reduction of its degree of water saturation. In parallel, E_{corr} increased moderately by ~100 mV and R_p increased by ~20 kΩ·cm^2 (Figure 5).

Soaking in tap water and subsequent chloride exposure, that is, partial immersion in 1 M NaCl solution, caused a decrease of E_{corr} by ~100–200 mV, a decrease of R_p by ~20–40 kΩ·cm^2, and a decrease of R_{el} by ~300 Ω for most of the mortar specimens (Figures 3, 5, and 6; Figures S1, S3, and S4). Specimen series FA-L-Cl exhibited similar decreases of E_{corr} and R_p, and a drop of R_{el} by ~100 Ω on chloride exposure (Figures 4 and S2). The decrease of the R_{el} is attributed to the penetration of Cl^- ions into the

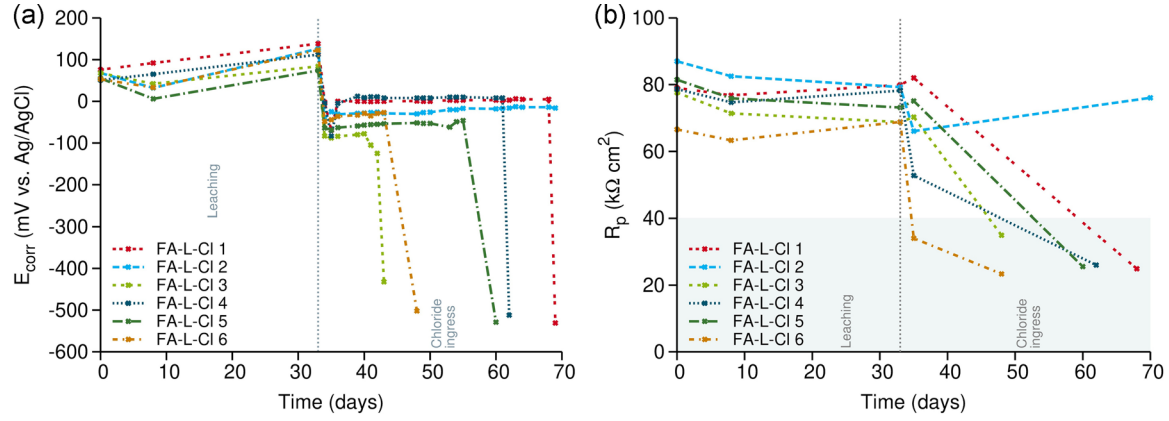

FIGURE 4 (a) Evolution of the open-circuit potential E_{corr} and (b) the polarization resistance R_p of the steel in the alkali-activated fly ash mortar exposed to leaching and chloride ("L-Cl") [Color figure can be viewed at wileyonlinelibrary.com]

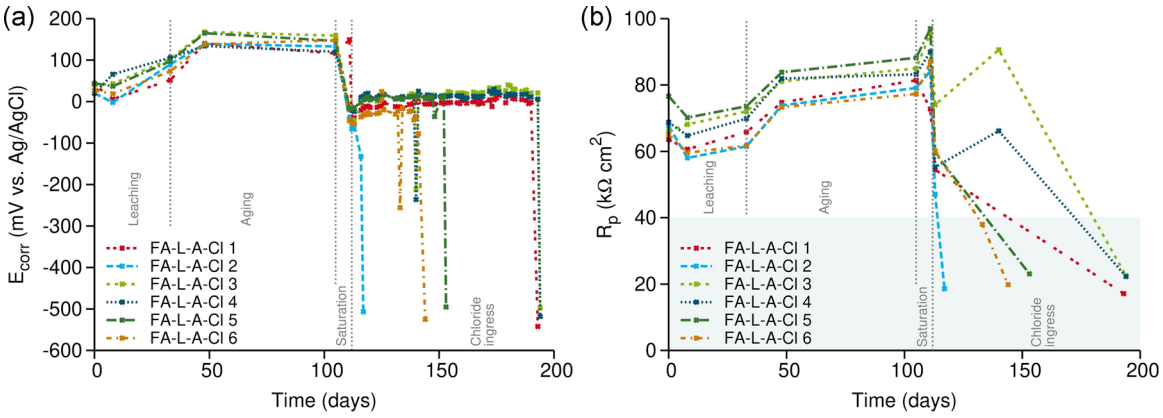

FIGURE 5 (a) Evolution of the open-circuit potential E_{corr} and (b) the polarization resistance R_p of the steel in the alkali-activated fly ash mortar exposed to leaching, aging, and chloride ("L-A-Cl") [Color figure can be viewed at wileyonlinelibrary.com]

mortar prisms, which reduces the resistivity of the mortars in surface-near regions; in addition, the uptake of water contributed to the reduction of the mortar resistivity for all specimen series except FA-L-Cl, which was already water-saturated before chloride exposure. The decrease of R_{el} changes the state of the electrochemical system and is, at least partly, responsible for the parallel decrease of the recorded values of E_{corr} and R_p.

With continuing chloride exposure, E_{corr} decreased further to values around −200 mV after approximately 50 days for the Portland cement mortar, while E_{corr} remained in the range 0 to −100 mV for most of the alkali-activated fly ash mortar specimens (Figures 3–6). The R_p values during chloride exposure of the alkali-activated fly ash mortar and the Portland cement mortar were comparable but tended to exhibit larger scatter for the former (Figures 3–6). R_{el} of the Portland cement mortar increased from ~200 to ~400 Ω during that period, indicating pore refinement due to continuing cement hydration, while R_{el} of the alkali-activated fly ash mortar remained approximately constant at ~100 Ω (Figures S1–S4).

The transition from passive to the active state of the steel was defined in this study as having occurred when E_{corr} decreased by at least 200 mV between successive measurements (i.e., within 1–2 days), and R_p recorded after that decrease was below 40 kΩ·cm^2 (cf. References[3,22]). For three of the Portland cement mortar specimens, the decrease of E_{corr} occurred less sudden (CEM-A-Cl 1 and CEM-A-Cl 5) or the decrease was <200 mV (CEM-A-Cl 3), but these were assumed to be in the active state as indicated by the evolution of their E_{corr} and R_p (Figure 6). For all specimens that were judged to be in the active state, visual inspection of the split mortar prisms and the embedded steel rebars confirmed that corrosion initiation had occurred, as evidenced by corrosion products on the steel surfaces (Figures S5–S28).

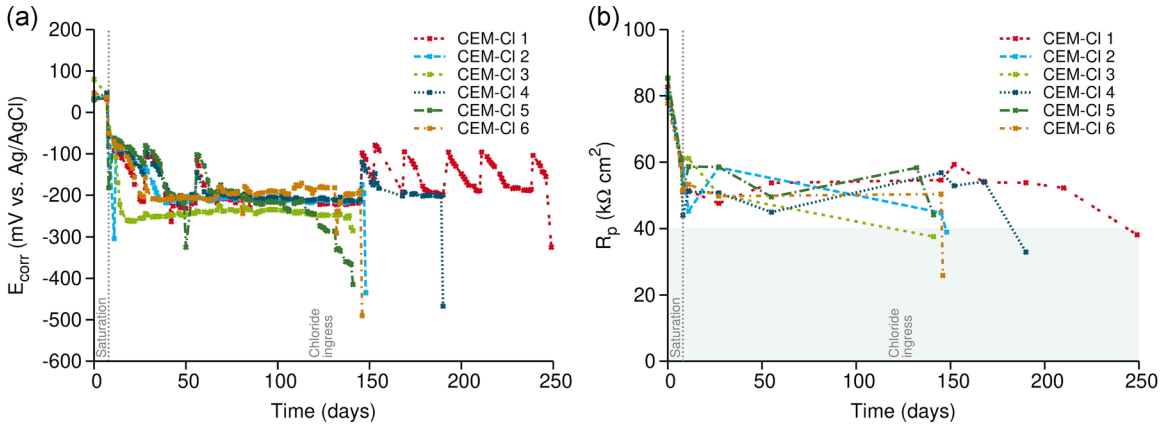

FIGURE 6 (a) Evolution of the open-circuit potential E_{corr} and (b) the polarization resistance R_p of the steel in the Portland cement mortar exposed to chloride ("Cl") [Color figure can be viewed at wileyonlinelibrary.com]

3.2 | Location of corrosion products and chloride contents

Most of the alkali-activated fly ash mortar specimens in which corrosion initiation was detected exhibited corrosion products adjacent to one of the two welding joints between the rebar and a stainless-steel wire (Figures 7, S5–S22; Table S1). On the contrary, visual inspection showed that corrosion initiation occurred randomly distributed over the steel surface in the Portland cement mortar (Figures 7, S23–S28; Table S1). Thus, according to recommended practice,[22] the median value of the chloride contents determined for the Portland cement mortar can be referred to as critical chloride content (c_{crit}), while this is not the case for the alkali-activated fly ash mortar.

The median values of the chloride contents (each chloride content being the average along the length of the original rebar position; see Section 2.2) that led to corrosion -initiation in the alkali-activated fly ash mortar under the different exposure conditions were FA-Cl: 0.55 wt% Cl wrtb; FA-L-Cl: 1.05 wt% Cl wrtb; FA-L-A-Cl: 0.35 wt% Cl wrtb (Figure 7). These values were of the same order of magnitude as, but consistently lower than, the critical chloride content in the Portland cement mortar (CEM-Cl: 1.21 wt% Cl wrtb; Figure 7). Because of preferential corrosion at welding joints, a direct comparison of the median chloride contents for the alkali-activated fly ash mortar with the c_{crit} of the Portland cement mortar is not warranted; nevertheless, some preliminary conclusions regarding the corrosion susceptibility of steel in the former may be drawn, as will be discussed below.

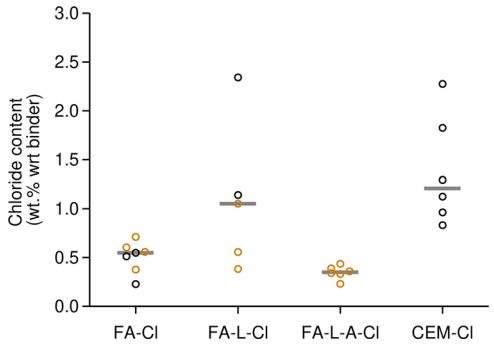

FIGURE 7 Scatter plot showing the chloride contents (average along the length of the original rebar position) at the time of steel corrosion initiation in the alkali-activated fly ash mortar and the Portland cement mortar. Yellow-ocher circles represent specimens in which corrosion had occurred in spatial proximity to the welding joint between the steel rebar and a stainless-steel wire; black circles represent specimens in which corrosion occurred closer to the middle of the steel rebar, that is, not in spatial proximity to the welding joint (see main text for additional details; individual values are listed in Table S1). The gray lines show the median chloride content for each mortar-exposure combination [Color figure can be viewed at wileyonlinelibrary.com]

3.3 | Corrosion experiments in solution

A possible explanation for the preferential corrosion initiation near the welding joints in the alkali-activated fly ash mortar could be that welding had affected the steel in proximity to the welding joint, making it more susceptible to corrosion. A higher corrosion susceptibility can be caused by alterations of the steel in the heat-affected zone, for example, thermal deformation stresses or induced microstructural and/or compositional heterogeneities, including recrystallization and grain growth.[23] The absence of preferential corrosion in the Portland cement mortar, however, shows that these hypothetical alterations would become effective only under conditions specific to the alkali-activated fly ash binder, that is, its pore solution composition and the resulting potential of the steel.

To test the possibility that preferential corrosion in the alkali-activated fly ash mortar was caused by effects of welding, rebars with stainless-steel wires welded to them, as used for the mortar experiments, and single stainless-steel specimens were exposed either to 1 M NaOH solutions, or to a 1 M NaOH solution and subsequently to a 1.7 M NaCl/1 M NaOH solution, and current density–potential curves recorded in these solutions. The open-circuit potentials of the stainless-steel specimens and the rebar-wire specimens were approximately −300 and −200 mV in the 1 M NaOH

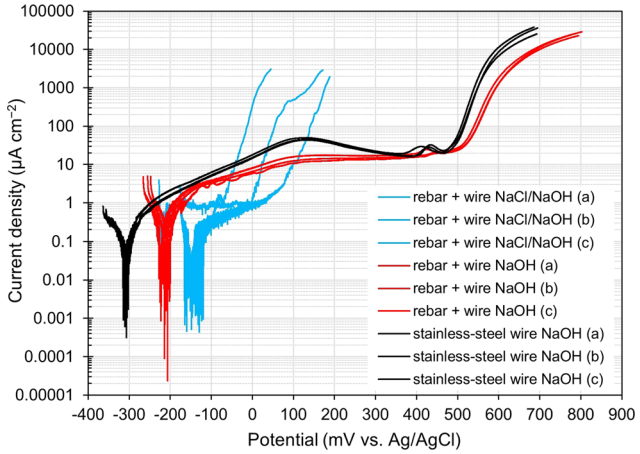

FIGURE 8 Current density–potential curves of stainless-steel wires (black curves) and rebars with stainless-steel wires welded to them (red curves) in 1 M NaOH solution, and rebars with stainless-steel wires welded to them in 1.7 M NaCl/1 M NaOH solution (blue curves) [Color figure can be viewed at wileyonlinelibrary.com]

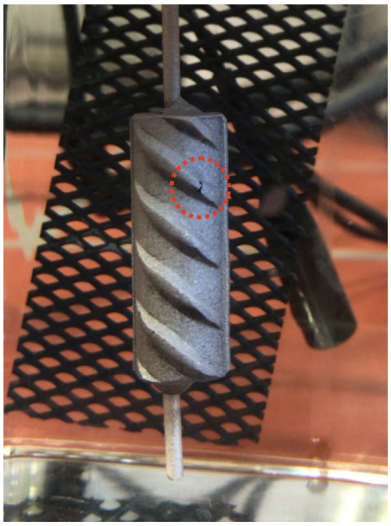

FIGURE 9 Photograph of a corrosion pit (marked with the red, dotted circle) on the surface of a rebar-wire specimen exposed to 1.7 M NaCl/1 M NaOH solution [Color figure can be viewed at wileyonlinelibrary.com]

solution, respectively, indicating a passive state for both. Both specimen series exhibited comparable current densities over the sampled potential range (Figure 8). As shown by the more negative E_{corr} of the stainless-steel specimens, the rebar forms the cathode in the rebar-wire system; a galvanic element with the carbon steel as the anode can thus be excluded.

In the 1.7 M NaCl/1 M NaOH solution, the open-circuit potential of the rebar-wire specimens was shifted to more positive potentials of approximately −150 mV, and the current density–potential curves exhibited pitting corrosion initiation potentials in the range approximately −75 to 50 mV (Figure 8). Visual inspection during exposure to the chloride-containing solution revealed that, in all rebar-wire specimens, pitting corrosion initiation almost exclusively occurred distant from the welding joint between the rebar and the stainless-steel wire, that is, outside the heat-affected zone, as illustrated in Figure 9. It is thus concluded that a higher corrosion susceptibility of the steel surface, caused by welding, was not the cause for the preferential corrosion near the welding joints in the alkali-activated fly ash mortar prisms.

3.4 | Steel–mortar interface in the alkali-activated fly ash mortar

As alterations of the steel surface due to welding were not at the origin of the preferential corrosion at the joints, another mechanism must underly its occurrence. The most economic explanation appears to be the preferential formation of corrosion-promoting defects such as air voids[8,24] at the welding joints in the alkali-activated fly ash mortar specimens, but not in the Portland cement mortar.

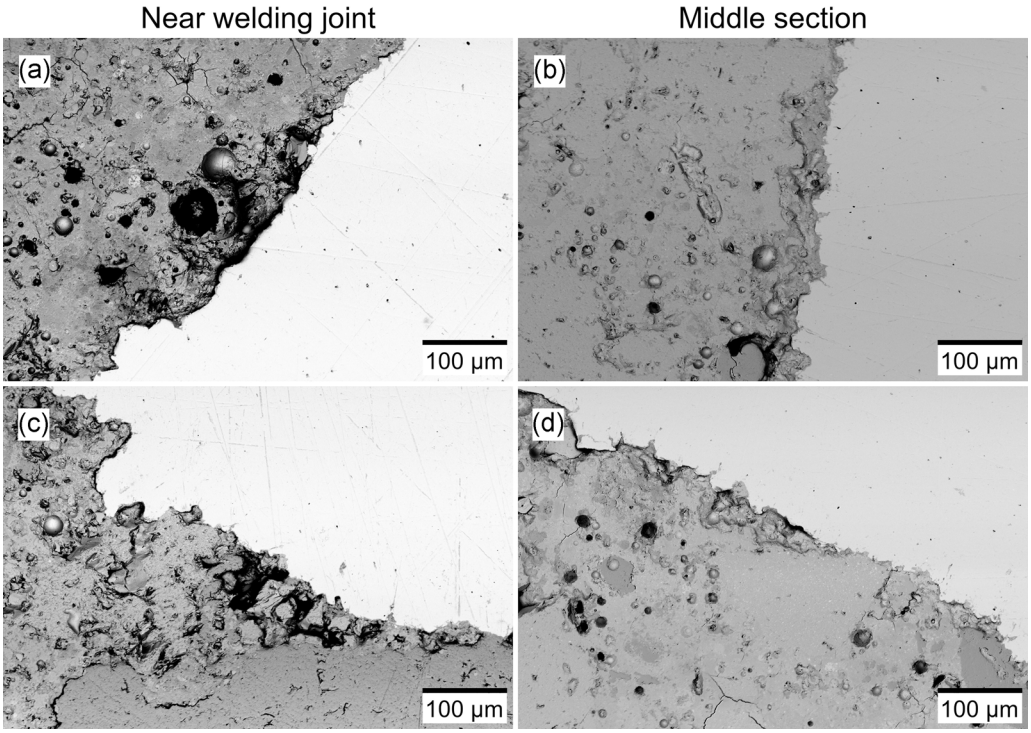

FIGURE 10 Scanning electron micrographs (backscattered electron mode) of the steel–mortar interface in an alkali-activated fly ash mortar in the region close to the rebar end, that is, close to (a,c) a welding joint and (b,d) in the central region of the mortar prism

A confirmation of this hypothesis was provided by SEM micrographs of the steel–mortar interface. Figure 10 illustrates that the interface between the alkali-activated fly ash mortar and the steel rebar was more porous in the region close to the welding joint than in the middle section of the mortar prisms. Generally, the steel–mortar interface in this mortar exhibited more and larger pores/voids and the mortar was detached from the steel along considerably longer segments in the region close to the welding joint than in the central region (cf. also Figure S29). The Portland cement mortar specimens generally exhibited less and smaller voids at the steel–mortar interface, and contrary to what was observed for the alkali-activated fly ash mortar, they exhibited no significant difference between the regions close to the welding joints and the central regions of the rebar (cf. Figure S30).

It is proposed that the preferential formation of defects close to the rebar ends in the alkali-activated fly ash mortars was caused by the interplay between eccentricities of the stainless-steel wires, movement of rebar and mortar during compaction (vibration), and the peculiar rheological characteristics of fresh alkali-activated materials, which make them generally less workable than Portland cement-based materials.[25,26] Further experiments are required to verify the validity and determine the range of applicability of the proposed mechanism. A major question is whether its occurrence is specific to the setup used in the present study or not, that is, whether a similar accumulation of defects can be expected for other sample geometries and rebar installations too.

4 | CONCLUSIONS

The open-circuit potentials and the polarization resistances of the carbon steel rebars were comparable in the alkali-activated fly ash mortar and the Portland cement mortar under the employed conditions; this was the case in both the passive and the active state. However, the polarization resistance tended to exhibit larger scatter over the observation period for the alkali-activated fly ash mortar, potentially impairing its usefulness as an indicator of corrosion initiation. A significant difference between the two materials was the higher ohmic resistance of the Portland cement mortar, compared with the alkali-activated fly ash mortar, presumably caused by a finer pore structure of the former. In addition, the ohmic resistance of the Portland cement mortar increased during chloride exposure due to continuing pore refinement, while this was not the case for the alkali-activated fly ash mortar.

The median values of the chloride contents leading to corrosion initiation in the alkali-activated fly ash mortar were in the range 0.35–1.05 wt% Cl wrtb, lower than what was found for the Portland cement mortar. The results for the alkali-activated fly ash mortar were influenced by preferential corrosion near welding joints at the steel rebars, caused by defects at the steel–mortar interface close to the joints. Even if it is assumed that the chloride contents obtained in the present study represent a conservative estimate of the critical chloride content in alkali-activated fly ash, the present results, taken together with the generally low chloride-binding capacity of low-Ca alkali-activated materials[27] and their comparatively high effective chloride transport coefficients,[13,21,27] indicate that concretes based on alkali-activated fly ash require particularly careful design, and possibly additional measures, to protect embedded steel reinforcement from corrosion in environments where the concretes are exposed to chlorides.

A systematic influence of leaching on the corrosion-initiating chloride content of the alkali-activated fly ash mortar could not be identified, but this is likely related to scatter and bias introduced by the preferential corrosion near welding joints. Leaching of alkali ions and the concomitant decrease of pH[19,20] is expected to further decrease c_{crit}[14] and would thus further increase the risk posed by chloride exposure. Additional research is required to quantify these risks and to develop corresponding design recommendations for concretes based on low-Ca alkali-activated binders.

The finding that preferential void formation and corrosion initiation occurred near welding joints in the alkali-activated fly ash mortar, but not in the Portland cement mortar, demonstrates that a number of differences between the properties of these materials (rheological properties in the fresh state, pore solution composition, etc.) can have an effect on which parameters determine corrosion initiation of embedded steel. The importance of spatially varying characteristics of the steel–concrete interface, including microstructural or chemical heterogeneities, has been highlighted recently for the case of conventional cement-based materials.[8,24] The present findings emphasize the need for a similar approach to alkali-activated materials, that is, studies dedicated to understanding the causes and the relative importance of various defects and microstructural alterations at the steel–concrete or steel–mortar interface in these materials.

ACKNOWLEDGMENTS

The authors thank Steffi Reinemann for assistance in carrying out the galvanostatic pulse measurements, Claudia Crasselt for help in performing the SEM analyses, and Shishir Mundra for valuable discussions. This study was funded by the AiF e.V. within the IGF program on behalf of the German Federal Ministry for Economic Affairs and Energy (project 18910 N/1 of the GfKORR e.V.).

CONFLICT OF INTERESTS

The authors declare that there are no conflict of interests.

ORCID

Gregor J. G. Gluth http://orcid.org/0000-0002-8951-7393
Gino Ebell http://orcid.org/0000-0002-6006-2460
Jürgen Mietz http://orcid.org/0000-0002-2878-7576

REFERENCES

[1] U. M. Angst, *Mater. Struct.* **2018**, *51*, 4.
[2] P. Ghods, O. B. Isgor, G. A. McRae, G. P. Gu, *Corros. Sci.* **2010**, *52*, 1649.
[3] U. M. Angst, B. Elsener, C. K. Larsen, Ø. Vennesland, *Corros. Sci.* **2011**, *53*, 1451.
[4] U. Angst, B. Elsener, C. K. Larsen, Ø. Vennesland, *Electrochim. Acta* **2011**, *56*, 5877.
[5] H. DorMohammadi, Q. Pang, P. Murkute, L. Árnadóttir, O. B. Isgor, *npj Mater. Degrad.* **2019**, *3*, 19.
[6] M. C. Alonso, M. Sanchez, *Mater. Corros.* **2009**, *60*, 631.
[7] U. Angst, B. Elsener, C. K. Larsen, Ø. Vennesland, *Cem. Concr. Res.* **2009**, *39*, 1122.
[8] U. M. Angst, M. R. Geiker, M. C. Alonso, R. Polder, O. B. Isgor, B. Elsener, H. Wong, A. Michel, K. Hornborstel, C. Gehlen, R. François, M. Sanchez, M. Criado, H. Sørensen, C. Hansson, R. Pillai, S. Mundra, J. Gulikers, M. Raupach, J. Pacheco, A. Sagües, *Mater. Struct.* **2019**, *52*, 88.
[9] S. Mundra, S. A. Bernal, M. Criado, P. Hlaváček, G. Ebell, S. Reinemann, G. J. G. Gluth, J. L. Provis, *RILEM Tech. Lett.* **2017**, *2*, 33.
[10] D. M. Bastidas, A. Fernández-Jiménez, A. Palomo, J. A. González, *Corros. Sci.* **2008**, *50*, 1058.
[11] C. Monticelli, M. E. Natali, A. Balbo, C. Chiavari, F. Zanotto, S. Manzi, M. C. Bignozzi, *Cem. Concr. Res.* **2016**, *80*, 60.
[12] C. Monticelli, M. E. Natali, A. Balbo, C. Chiavari, F. Zanotto, S. Manzi, M. C. Bignozzi, *Cem. Concr. Res.* **2016**, *87*, 53.
[13] M. Babaee, A. Castel, *Cem. Concr. Res.* **2018**, *111*, 56.
[14] S. Mundra, M. Criado, S. A. Bernal, J. L. Provis, *Cem. Concr. Res.* **2017**, *100*, 385.
[15] U. M. Angst, B. Elsener, *Sci. Adv.* **2017**, *3*, e1700751.
[16] M. Criado, J. L. Provis, *Front. Mater.* **2018**, *5*, 34.
[17] C. J. Newton, J. M. Sykes, *Corros. Sci.* **1988**, *28*, 1051.
[18] B. Elsener, O. Klinghoffer, T. Frolund, E. Rislund, Y. Schiegg, H. Böhni, Int. Conf. Repair of Concrete Structures: From Theory to Practice in a Marine Environment, Svolvær, Norway, 28–30 May, 1997, pp. 391–400.
[19] R. R. Lloyd, J. L. Provis, J. S. J. van Deventer, *Cem. Concr. Res.* **2010**, *40*, 1386.
[20] P. Hlaváček, S. Reinemann, G. J. G. Gluth, G. Ebell, J. Mietz, Int. Conf. Sustainable Materials, Systems and Structures (SMSS 2019), Rovinj, Croatia, 20–22 March, 2019, Vol. 1, pp. 118–124.
[21] G. J. G. Gluth, P. Hlaváček, S. Reinemann, G. Ebell, J. Mietz, *MATEC Web Conf.* **2018**, *199*, 02025.
[22] U. M. Angst, C. Boschmann, M. Wagner, B. Elsener, *J. Vis. Exp.* **2017**, e56229.
[23] J. R. Davis, *Corrosion of Weldments*, ASM International, Materials Park, OH **2006**, pp. 1–10.
[24] U. M. Angst, M. R. Geiker, A. Michel, C. Gehlen, H. Wong, O. B. Isgor, B. Elsener, C. M. Hansson, R. François, K. Hornborstel, R. Polder, M. C. Alonso, M. Sanchez, M. J. Correia, M. Criado, A. Sagüés, N. Buenfeld, *Mater. Struct.* **2017**, *50*, 143.
[25] M. Criado, A. Palomo, A. Fernández-Jiménez, P. F. G. Banfill, *Rheol. Acta* **2009**, *48*, 447.
[26] A. Favier, J. Hot, G. Habert, N. Roussel, J.-B. d'Espinose de la Caillerie, *Soft Matter* **2014**, *10*, 1134.
[27] A. Noushini, A. Castel, J. Aldred, A. Rawal, *Cem. Concr. Compos.* **2020**, *105*, 103290.

SUPPORTING INFORMATION

Additional supporting information may be found online in the Supporting Information section.

How to cite this article: Gluth GJG, Ebell G, Hlaváček P, Mietz J. Chloride-induced steel corrosion in alkali-activated fly ash mortar: Increased propensity for corrosion initiation at defects. *Materials and Corrosion*. 2020;71:749–758. https://doi.org/10.1002/maco.202011541